Feasibility study for wrap-buoy assisted wet-tow and stepwise installation of mono-bucket foundation for 15 MW offshore wind turbine

Ikjae Lee and Moohyun Kim[*]

Department of Ocean Engineering, Texas A&M University, College Station, TX, 77845, USA

Abstract. An innovative concept for wet-transportation and stepwise installation of mono-bucket foundation for 15 MW offshore wind turbine is proposed. Case studies for two different mono-bucket and wrap-buoy dimensions are conducted and their hydrostatic and hydrodynamic performances are compared for both wet-towing and lowering operations. The intact stability and transient responses are analyzed in detail for various stages of lowering operation. Wave-induced motion statistics during wet tow in sea state 4 (highest operational window) are checked. The proposed concept is found to be feasible and can be an alternative cost-effective solution without using heavy-lift crane vessel in practice.

Keywords: acoustic shackle; intact stability; segmented wrap buoy; stepwise installation; transient response; vertical wet tow; without crane vessel

1. Introduction

The importance of offshore wind turbine for supplying green energy has been widely recognized among many countries during the past decade. Among the installed offshore wind turbines, the fixed monopile type foundation has mostly been used in relatively shallow water regions. Their sizes are also growing since larger turbines have higher efficiency and more advantages. The standard NREL fixed foundation for 15 MW turbine consists of a 10 m diameter, 75 m long, 1318ton monopile (Gaertner *et al.* 2020) that is driven 45 m into the seabed (See Fig. 1). Mono-pile foundation has to be driven into soil by impact hammers which generate unwanted noises to potentially disturb sea mammals. The presence of rock layers can also be a concern for deep pile penetration. In this regard, other types of fixed foundations, such as gravity foundation (Esteban *et al.* 2015, Esteban *et al.* 2019) and suction-bucket foundation (Abdel-Rahman and Achmus 2006, Feld 2001, Wang *et al.* 2019, Jeong *et al.* 2021) are also considered due to no need of hammering, wider adaptability to various soil conditions, and relatively low construction/installation cost (Lian *et al.* 2012, Zhang *et al.* 2015). In this paper, an innovative wet-towing and installation methods of suction bucket foundations holding 15 MW NREL wind turbine (Wu and Kim 2021) are investigated.

The standard methodology for the installation of fixed-type foundations is to use installation vessels with a high-capacity crane. However, its safety, low availability, high day rate are

---

*Corresponding author, Professor, E-mail: m-kim3@tamu.edu

challenging issues for large-scaled (e.g., 15 MW) offshore wind turbines (Jiang 2021). Alternatively, a dedicated transportation and installation vessel was devised for the bucket foundation by Zhang *et al.* (2015). In the present study, authors developed an innovative concept for the wet-towing and installation of the mono-bucket foundation without using HLVs.

To achieve the goal, a set of segmented wrap buoys are attached around the sidewall of the bucket foundation to secure hydrostatic stability while being towed out by tugboats to the installation site. At the installation site, the bucket foundation is gradually lowered by disconnecting those wrap buoy segments one-by-one in a stepwise manner. The wrap buoys are released by remote control through acoustic signals (Sundt *et al.* 2009, Fiorentino *et al.* 2019). The capacity of acoustic release shackle ranges from 25-300tonne (e.g., Applied Acoustic Engineering Ltd.). The developed wet-tow and installation concept for suction-bucket foundation seems much simpler and more cost-effective than those of typical gravity-base foundations for which significant amount of solid ballast has to be applied (Esteban *et al.* 2015).

The feasibility study for the wet-tow and sequential installation of circular cylindrical mono-bucket foundation is performed in this paper. The case studies include two different mono-bucket dimensions, tall/slender and shallow/wider (Aubeny 2022, Aubeny and Aldawwas 2022), that can support the standard 15 MW turbine of Fig. 1. The corresponding intact stability and dynamic responses during wet-towing and step-wise installation by sequentially disconnecting segmented wrap buoys are analyzed. Specifically, intact stability and transient dynamics when disconnecting respective wrap-buoy segments are investigated in detail for each stage.

In section 2, the proposed concept is explained in detail, and several initial hydrostatic and hydrodynamic analyses and relevant theoretical backgrounds are briefly described. In section 3, calculation results for two selected mono-bucket dimensions are presented and discussed, and then we conclude the paper with concluding remarks in section 4.

Fig. 1 Mono-pile concept of 15 MW offshore wind turbine (Gaertner *et al.* 2020). The mono bucket foundation for the same 15 MW turbine is considered
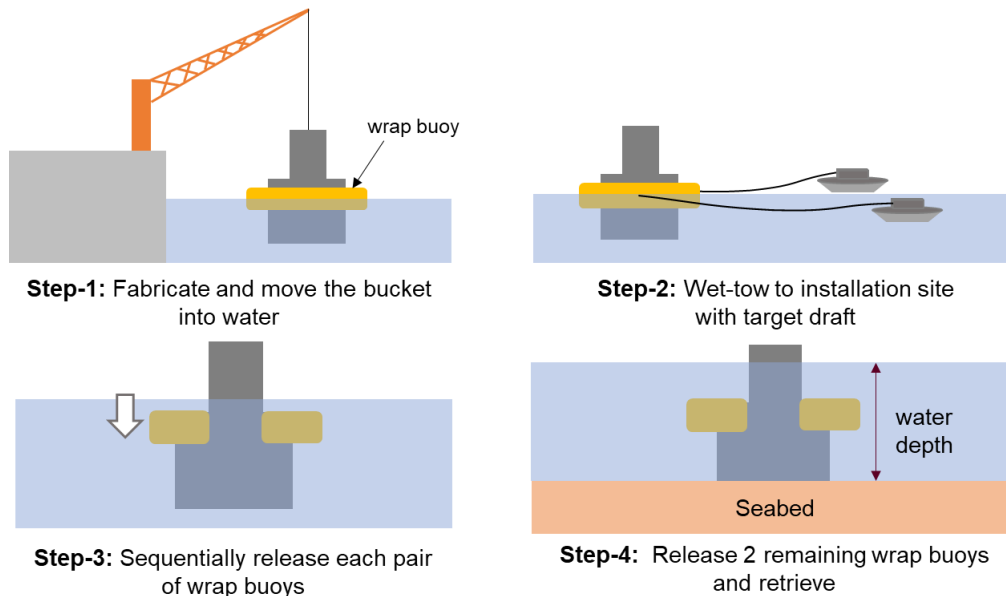
Fig. 2 Summarized procedure for transportation and installation
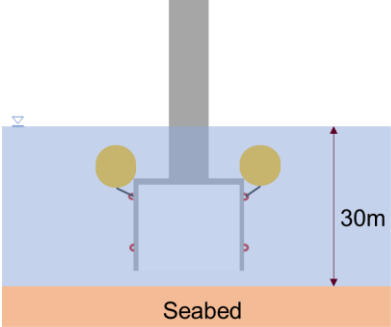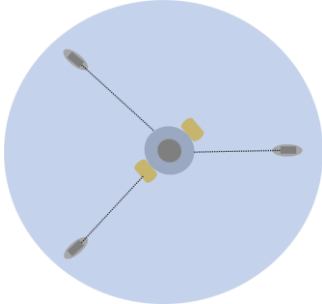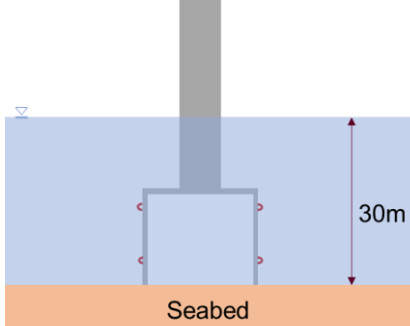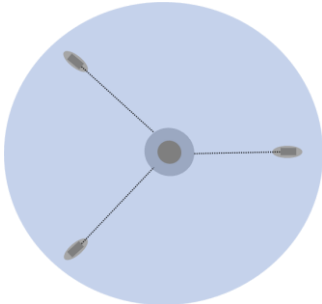
2. Wet-tow and stepwise installation

The overall procedure of the developed method for the wet-towing and sequential installation are summarized and illustrated in Fig. 2. The bucket foundation was sized for the same NREL 15 MW reference turbine (Fig. 1) at the same water depth of 30 m. The seabed of installation location is assumed to be pretreated to be flat.

- Step-1: All components of bucket foundation including assisting wrap-buoy units are assembled at quayside land. Then, the bucket foundation is placed into the water by using a land crane. During the loadout, the wrap buoys enable the foundation to be afloat. The segmented wrap buoys are connected to the upper and lower bucket pad-eyes at both ends through acoustic shackles and short cables. The acoustic shackles are to be disconnected remotely by using acoustic signal during the installation.

- Step-2: Tow the floating unit to the designated installation site with the wet tow draft. The floating foundation is towed by 3 tugboats via towing lines to a designated installation site.

- Step-3: At the installation site, three tugboats position the foundation to be located directly above the target seabed. Once the foundation is positioned, lower acoustic shackles of all buoys are released by remote control to elevate the buoyancy center while initially lowering the bucket foundation. Then, each pair of segmented wrap buoys is remotely released one-by-one in a symmetric manner by acoustic signal. After each pair of wrap buoys is released, the corresponding loss of buoyancy is compensated by the increased buoyancy of upper tower by deeper submergence. Then, the foundation reaches a new weight-buoyancy equilibrium draft. The remote releasing processes are repeated until the lowest part of the foundation lands at the seabed. During the sequential lowering process, the static stability can be maintained. The additional stability can also be provided by the tensions of 3-tug-boat cables.

Table 1 Lowering operation stages: Sequential view sketches

Stage	Sectional view	Birds-eye view	Description
1			At the installation site, position the bucket by three tugs to be at the right above of target seabed.
2			Release the lower shackles, so that wrap buoys are elevated, and the draft is increased.
3			Release two wrap buoys. (Total 6 wrap buoys)
			Release two more wrap buoys. (Total 4 wrap buoys)

Table 1 Continued

5			Release two more buoys. From this step, the buoys are fully submerged, and the buoyancy is increased by the increased monopile submergence. (Total 2 wrap buoys)
6			Release two more buoys. and the bucket is landed at the target seabed. During the lowering operation, the bucket's position is adjusted by three tugs.

- Step-4: After the foundation is completely landed on the seabed, all the disconnected wrap buoys will be afloat and retrieved by tugboats for reuse. Tugboats are to bring those retrieved wrap-buoys to the port for the next operation.

2.1 Sequential views for installation

Schematic views for the entire installation process in the step-3 of Fig. 2 are detailed in Table 1. All the lowering stages are illustrated with sectional and bird-eye views together with descriptive explanation for each stage. As illustrated, the bucket foundation is to be positioned right above a target seabed by three tugs using towing lines at the site. Then the foundation is lowered down in a stepwise manner by remotely releasing acoustic shackles one-by-one in a symmetric way until it is safely landed at the target seabed within tolerance. The bucket maintains its draft at pre-calculated equilibrium positions (Stages 1-5), at each of which the weight of the foundation is in equilibrium with the buoyancy force. At every equilibrium draft, the corresponding upright stability needs to be checked. In the meantime, the cables from three tugs can provide additional stability and safety. The following hydrostatic and hydrodynamic analyses were performed:
- Intact stability
- Wave-induced motion statistics in wet tow
- Dynamic simulation in lowering operation
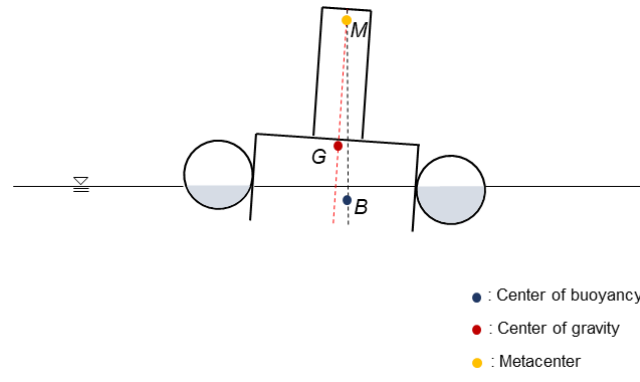- Overturning moment after seating on seabed

Fig. 3 A sketch for intact stability in wet tow

2.2 Intact stability

In the transportation and installation phases, the floating bucket foundation needs to resist overturning moment for rolling and pitching due to waves, currents, and winds. The metacentric height (GM) is a good indication of the stability of a floating body. The GM is the distance from the center of gravity to the metacenter of a floating body (See Fig. 3) and positive GM means that the system is stable against the overturning moment. The GM can be calculated by

$$\overline{GM} = z_B - z_G + \frac{I_{xx}}{\nabla} \qquad (1)$$

where ∇ is the displaced volume, I_{xx} is the second moment of waterplane area, z_B and z_G are center of buoyancy and gravity, respectively.

2.3 Wave-induced motion statistics

Wave spectrum

In the present study, JONSWAP wave amplitude spectrum is selected (Hasselmann and Olbers 1973)

$$S_\zeta(\omega) = (1 - 0.287 \ln \gamma)(5/16) H_S^2 \omega_p^4 \omega^{-5} e^{-b\omega_p^4/\omega^4} \gamma^a \quad \text{with} \quad a = e^{-\left(\omega - \omega_p\right)^2 / 2\omega_p^2 \sigma^2} \qquad (1)$$

where ω_p is peak frequency and H_s is significant wave height, γ is the peak enhancement factor, $b = 1.25$, σ is spectral width parameter, $\sigma = 0.07$ if $\omega \leq \omega_p$, otherwise $\sigma = 0.09$.

The wave spectra for different tow speeds are generated based on the encounter-frequency conversion

$$S_\zeta(\omega_e) = S_\zeta(\omega)(\frac{C_g}{C_g - U \cos \beta}) \quad \text{with} \quad \omega_e = \omega - kU \cos \beta \qquad (2)$$

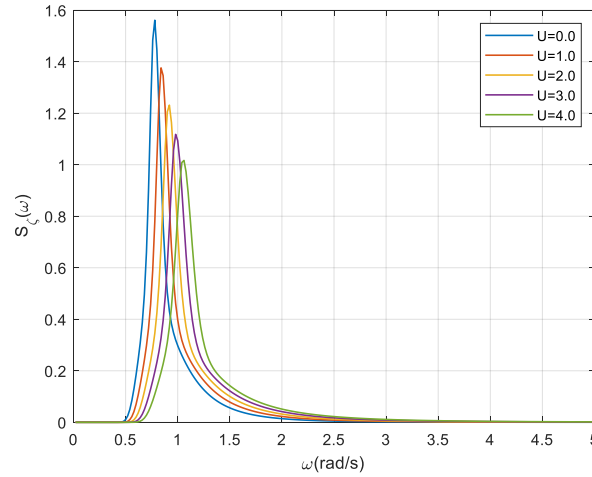Fig. 4 JONSWAP Wave spectrum with different tow speeds

Table 2 Met-ocean parameters for sea-state 4

$T_p(s)$	$H_s(m)$	γ	$\beta(°)$	$U(m/s)$
8.1	2.5	3.3	180	0,1,2,3,4

where the group velocity $C_g = \frac{1}{2}C_p(1+\frac{2kh}{\sinh 2kh})$; here, the phase velocity $C_p = \sqrt{\frac{g}{k}\tanh kh}$. ω_e is the encounter frequency determined by tow speed, U, and wave heading angle, β. Met-ocean parameters for sea state 4 are given in Table 2 and the generated wave spectra are shown in Fig. 4. The peak enhancement factor is chosen as 3.3 that has been used for many engineering works but it varies according to target locations (Mazzaretto *et al*. 2022).

<u>Equation of motion & Response amplitude operators (RAOs)</u>

The equation of motion in the frequency-domain is given by

$$[(-\omega_e^2(M_{ij}+A_{ij})+C_{ij})+i\omega_e(B_{ij}^V+B_{ij}^R)]\xi_j = X_i \qquad (4)$$

Where M_{ij} and A_{ij} are inertia (mass) and added inertia, B_{ij}^V and B_{ij}^R are viscous (linear equivalent) and radiation damping, C_{ij} is hydrostatic stiffness, X_i is wave exciting force and moment. Subscripts $i=1-6$ and $j=1-6$ mean respective modes of 6DOF motions.

To calculate frequency dependent added mass, radiation damping and wave excitations in (4) a commercial 3D diffraction/radiation panel program WAMIT is used (Lee 1995). For simplicity, the tow-line-induced additional effects are neglected. Since tugboats are small, their hydrodynamic interaction effects are not considered either. The linear equivalent viscous damping is additionally inputted to the program with 3% and 5% of critical damping for heave and pitch, respectively.

Based on Eq. (4), heave and pitch motion RAOs are calculated as

$$\left|RAO_{\xi_i}\right| = \left|\xi_i\right| = \frac{\left|X_i\right|}{\sqrt{\left(-\omega_e^2(M_{ii}+A_{ii})+C_{ii}\right)^2 + \omega_e^2\left(B_{ii}^V+B_{ii}^R\right)^2}} \ , \quad i = 3,5 \tag{5}$$

Motion spectrum and motion statistics

Motion spectrum and their statistics are estimated based on the input wave spectrum and RAOs. In the linear time-invariant system, motion spectrum can be obtained as $S_{\xi_i}(\omega_e) = S_\zeta(\omega_e)\left|RAO_{\xi_i}\right|^2$. Based on them, several wave and motion statistics are estimated as follows:

- $\sigma = \sqrt{m_0}$: Standard deviation
- $\eta_S = 2\sqrt{m_0}$: Significant wave(motion) amplitude
- $\eta_E = \sigma_\eta\sqrt{2\ln\left(10800/T_2\right)}$: The most probable extreme wave(motion) amplitude for 3 hours

where η is either ζ (wave) or ξ_i (motion amplitude for i-mode), $m_i = \int_0^\infty (\omega_e)^i S(\omega_e)d\omega_e$ and mean wave period $T_2 = 2\pi\sqrt{m_0/m_2}$.

2.4 Lowering operation

Dynamic simulations in the respective lowering steps have been carried out. Each disconnection step causes transient up-and-down motions of the floating system until equilibrium draft is set. As shown in Table 1, the mono-bucket foundation is lowered down in a stepwise manner i.e., two segmented wrap buoys are released at a time in a symmetrical manner by the acoustic signal which commands the acoustic shackles to be released. Owing to the sudden decrease of buoyancy force by the disconnected wrap buoys, the foundation starts to fall until the buoyancy deficiency is compensated by the increased submergence of upper tower. During this short period, transient heave motions of the system occur. At the end of each transient response, the bucket reaches a new equilibrium position at which the buoyancy is balanced by the weight. This process is repeated until the bucket foundation is safely landed on the seabed. The transient heave responses and velocities are estimated from the separate time-dependent transient motion analysis for the respective stages. The worst scenario at which GM becomes minimum is selected among all the lowering steps for more detailed analysis. A schematic view for the lowering operation is illustrated in Fig. 5. In the figure, $d(t)$ is instantaneous draft from the mean water level ($z = 0$) to the bucket's bottom.

Transient equation of motion

The equation of transient motion is given by

$$(M + A_{33}(\infty))\ddot{z}(t) + C_D^*\dot{z}\left|\dot{z}\right| + \int_{-\infty}^t K_{33}(t-\tau)\dot{z}(\tau)d\tau + C_{33}z(t) = B - W + T \tag{6}$$

where

- $A_{33}(\infty)$ is the infinite frequency added mass in heave direction.
- $C_D^* = 0.5\rho(C_{D,n}A_{F,z} + C_{D,t}A_{Wet})$; ρ is the water density, $C_{D,n}$ and $C_{D,t}$ are drag coefficients for normal and tangential direction, and $A_{F,z}$ and A_{Wet} are the frontal area of bucket and wrap buoys projected to xy-plane and wetted area of bucket, respectively.
- $C_{33} = \rho g A_{WP}$; A_{WP} is the waterplane area.
- K_{33} is the retardation function standing for memory effect of radiation damping. It can be obtained from the cosine Fourier transform of radiation damping.
- B and W are buoyancy and gravity forces, and T is the vertical component of tension from towing lines.

The three-dimensional hydrodynamic coefficients need to be calculated from the 3D diffraction/radiation program. Considerable radiated waves are expected during the initial stage of lowering operation due to the presence of wrap buoys particularly when it is at or near the free surface. In fact, the variation of radiation damping with the change of draft needs to be incorporated. Also, the influence of trapped water inside the bucket is found to be significant, which results in high added mass that amounts to about 4-6 times of the foundation's mass according to the present numerical tests. On the other hand, drag coefficient, $C_{D,n}$=2.5, of the bucket is selected based on experimental data by Huang *et al.* (2010) and Det Norske Veritas guideline (2000). Moreover, the skin friction coefficient, $C_{D,t}$, is set as 0.008 based on the recommended value for a suction anchor in OrcaFlex (Orcina Ltd.). The tensile forces, T, from towing lines of three tugboats are assumed to be 100-200kN that is reasonable considering the general capacity of bollard pulls of tugs. The corresponding variation of tension by transient motions are assumed to be much smaller than the applied static tension. The main concern in the stepwise lowering operation is the maximum overshoot motion amplitude and velocity that occur immediately after the wrap-buoy is disconnected especially at the last lowering stage of the foundation, for which the bucket bottom is close to the seabed. The cable tensile forces can be a help in the last lowering stage close to seabed. The cable tensions are expected to be adjustable by changing tug-boat positions or cable winch. For the numerical simulation, Runge-Kutta Gill method is adopted for the time-domain solutions (Weisstein).

Let $y = \dot{z}$, then the Eq. (6) can be rewritten as a state-space equation

$$\dot{\mathbf{y}} = \left\{ \begin{array}{c} \dot{z} \\ \dot{y} \end{array} \right\} = \left\{ \begin{array}{c} y \\ \dfrac{1}{M + A_{33}(\infty)}\left(-W + B - C_{33}z - C_D^* y|y| - \int_{-\infty}^{t} K_{33}(t-\tau)y(\tau)d\tau\right) \end{array} \right\} \quad \text{with} \quad \mathbf{y}(0) = \left\{ \begin{array}{c} 0 \\ 0 \end{array} \right\} \qquad (7)$$

where the heave retardation function $K_{33}(t) = \dfrac{2}{\pi}\int_0^{\infty} B_{33}(\omega)\cos(\omega t)d\omega$; $B_{33}(\omega)$ is frequency-dependent heave radiation damping. It should be noted that the hydrodynamic coefficients are for zero towing speed.

The discretized equation can be written as

$$\mathbf{y}_{n+1} = \mathbf{y}_n + \frac{1}{6}[\mathbf{k}_1 + (2-\sqrt{2})\mathbf{k}_2 + (2+\sqrt{2})\mathbf{k}_3 + \mathbf{k}_4] + O(h^5) \qquad (8)$$
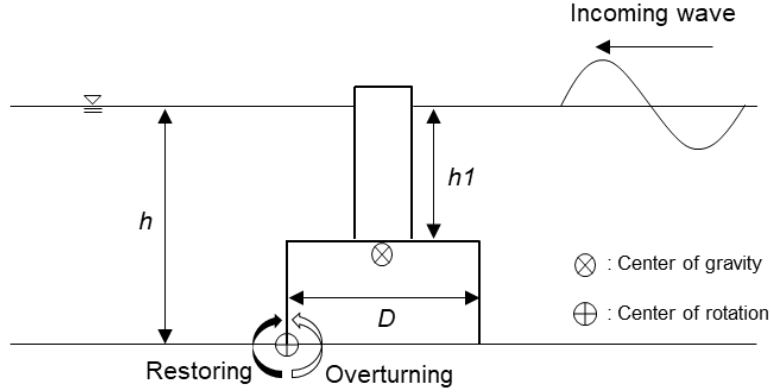
Fig. 6 A sketch for a seabed landed bucket subjected to the overturning moment

$$
\text{where }
\begin{cases}
\mathbf{k}_1 = \Delta t \mathbf{f}(t_n, \mathbf{y}_n) \\
\mathbf{k}_2 = \Delta t \mathbf{f}(t_n + \Delta t/2, \mathbf{y}_n + \mathbf{k}_1/2) \\
\mathbf{k}_3 = \Delta t \mathbf{f}(t_n + \Delta t/2, \mathbf{y}_n + (-1+\sqrt{2})\mathbf{k}_1/2 + (1-\sqrt{2}/2)\mathbf{k}_2/2) \\
\mathbf{k}_4 = \Delta t \mathbf{f}(t_n + \Delta t, \mathbf{y}_n - (\sqrt{2}/2)\mathbf{k}_2 + (1+\sqrt{2}/2)\mathbf{k}_3)
\end{cases}
; \quad \Delta t \text{ is the time step increment.}
$$

$$
\text{with } \mathbf{f}(t, \mathbf{y}_n) = \left\{
\begin{array}{c}
y_n \\
\dfrac{1}{M + A_{33}(z_n)} \left[-W + B - C_{33}z_n - C_D^* y_n |y_n| - \displaystyle\sum_{i=0}^{n} K_{33}(t_n - t_i, z_n) y_i \Delta t \right]
\end{array}
\right\}
$$

During the lowering simulation, the body position keeps changing and so are the added mass of infinite frequency and radiation damping coefficients (or retardation functions). Therefore, they are calculated for several drafts and interpolated by 3rd order Lagrange interpolating function as

$$
A_{33}(z) = \sum_{i=0}^{3} A_{33}(\infty, d_i) N_i(z), \quad K_{33}(t - \tau, z) = \sum_{i=0}^{3} K_{33}(t - \tau, d_i) N_i(z), \quad i = 0,1,2,3 \tag{9}
$$

with

$$
N_i(z) = \prod_{\substack{0 \le j \le 3 \\ i \ne j}} (z - z_j)/(z_i - z_j) \quad \text{with} \quad z_i = d_i - d_0 \tag{10}
$$

where the shape functions, N_i, interpolate the added mass and retardation functions with reference to four pre-selected drafts, d_i; here, d_0 is the lowest draft whereas d_3 the deepest.

In this regard, the transient-motion simulation can be considered as body-nonlinear simulation (Jang and Kim 2019).

Maximum overturing moment

The maximum overturning moment is estimated when the bucket is landed at the seabed but not penetrated into the soil yet. As mentioned earlier, sea state-4 is assumed, where the significant wave

height is 2.5 m and peak period is 8.1s. The maximum overturning moment for the most probable extreme wave height in the sea state 4 is calculated. The stability is evaluated based on restoring moment due to self-weight of the mono-bucket against the wave-induced overturing moment. A schematic view is illustrated in Fig. 6.

The strip-based Morison's force and overturning moment are given by

$$dF = \rho \frac{\pi D^2}{4} C_M a(t)dz + 0.5\rho D C_D u(t)|u(t)|dz \quad \text{and} \quad dM = (z+h)dF \tag{3}$$

with time-varying water particle velocity and accelerations along the depth:

$$u = \frac{\pi H}{T} \frac{\cosh k(z+h)}{\sinh kh} \sin(kx - \omega t) \quad \text{and} \quad a = -\frac{2\pi^2 H}{T^2} \frac{\cosh k(z+h)}{\sinh kh} \cos(kx - \omega t).$$

where C_M and C_D are inertia and drag coefficients, h is the water depth, H is wave height, T is wave period, k is wavenumber, ω is wave frequency.

The inertia and drag coefficients are determined based on KC (Keulegan-Carpenter) number and oscillatory Reynolds numbers. Based on the depth-averaged KC and Reynolds numbers, the inertia and drag coefficients of $C_M = 2.0$ and $C_D = 0.6$ are selected for the strip of cylindrical shape (Journée and Massie 2001). The most probable extreme wave height for 3 hours is approximately twice of the given significant wave height (=2.5 m), i.e., $H_E \approx 5m$. Applying the peak wave frequency with the most probable extreme wave height, the corresponding time-varying wave-induced overturing moment can be found as follows

$$
\begin{aligned}
M_{over} &= M_I \cos\omega t + \sin\omega t|\sin\omega t| \\
&= \left(\frac{2\pi^2 H_E}{T^2 \sinh kh}\right)\left[C_{I,mono}^* \int_{-h_1}^{0} f(z)dz + C_{I,bucket}^* \int_{-h}^{-h_1} f(z)dz\right]\cos\omega t \\
&\quad + \frac{1}{2}\left(\frac{\pi H_E}{T\sinh kh}\right)^2\left[C_{D,mono}^* \int_{-h_1}^{0} g(z)dz + C_{D,bucket}^* \int_{-h}^{-h_1} g(z)dz\right]\sin\omega t|\sin\omega t|
\end{aligned}
\tag{12}
$$

where $f(z) = (z+h)\cosh k(z+h)$ and $g(z) = (z+h)(1+\cos 2k(z+h))$; h and h_1 are in Fig. 6.

Then, the maximum overturning moment can be calculated by

$$\frac{dM_{over}}{dt} = -\omega M_I \sin\omega t + 2\omega M_D \cos\omega t|\sin\omega t| = 0 \tag{13}$$

Since M_I is much greater than $2M_D$ in the present bucket cases, when $\sin\omega t = 0$, the overturning moment has a maximum, i.e., $M_{over,\max} = M_I$.

On the other hand, the restoring moment by the wet weight can be calculated by

$$M_{res} = 0.5DW \tag{14}$$

where D is bucket's diameter, and W is the structural wet weight.

The stability of the system can be checked by the ratio of the maximum overturning moment over the restoring moment, i.e., $\mu = M_{over,\max}/M_{res}$. If $\mu < 1$, the system is stable against the

overturning moment. Alternatively, the wave-induced inertia force can be more accurately calculated by the 3D diffraction panel program WAMIT. Then the above formulas can be compared with the diffraction calculation. The overturning moment can be calculated by WAMIT as

$$
\begin{aligned}
M_{over,\max} &= 0.5H_E \left| -i\omega\rho \int_{S_{wet}} \varphi_D \mathbf{j} \cdot ((\mathbf{r} - \mathbf{r}_{C.R.}) \times \mathbf{N}dS) \right| \\
&= 0.5H_E \left| -i\omega\rho \int_{S_{wet}} \varphi_D N_5 dS - i\omega\rho h \int_{S_{wet}} \varphi_D N_1 dS + 0.5i\omega\rho D \int_{S_{wet}} \varphi_D N_3 dS \right| \\
&= 0.5H_E \left| X_5 + hX_1 - 0.5DX_3 \right|
\end{aligned}
\tag{15}
$$

Where H_E (=5 m) is the most probable extreme wave height, $\omega_p (= 2\pi/T_p)$ is the peak angular frequency, φ_D is the diffraction velocity potential in complex value, $\mathbf{j} = (0,1,0)$ is a unit vector along the axis of overturning moment, $\mathbf{r} = (x, y, z)$ is a coordinate vector from origin of the global cartesian coordinate system, $\mathbf{r}_{C.R.} = (-0.5D, 0, -h)$ is the center of rotation from the origin in Fig. 6; h is the water depth, and D is the bucket's diameter. $\mathbf{N} = (N_1, N_2, N_3)$ is the normal vector over the wetted surface, and $\mathbf{r} \times \mathbf{N} = (N_4, N_5, N_5)$ is generalized normal vector for rotational motion. Also, X_1 and X_3 are exciting forces in surge and heave, and X_5 is pitch exciting moment given in Eq. (4). All the exciting forces and moment are normalized by incident wave amplitude.

3. Case studies

3.1 Principal dimensions of slender and wide bucket foundations

In the present study, we performed feasibility studies for two different (slender and wide) mono-bucket dimensions. The ratio of bucket's sidewall length to diameter, *L/D*, is 1.0 and 0.5, respectively. These are two extreme cases of bucket design for the NREL 15MW turbine based on a series of rigorous soil-structure interaction analysis (Aubeny 2022, Aubeny and Aldawwas 2022). The principal dimensions of the mono-buckets and corresponding wrap buoys are given in Table 3, and the corresponding figures are illustrated in Fig. 7.

3.2 Case study-1: Slender bucket L/D = 1.0

Intact stability
Based on the formula given in (1), the metacentric heights are calculated for all stages of lowering operation as given in Table 4. During the wet tow, the center of the wrap buoy is located at 11 m from the bucket keel. As shown below, the present dimension (*L/D=1.0*) has positive GMs at all stages, which indicates that the system is stable during the whole stage of towing and installation. As three tugboats maintain their positions and provide additional tensions via towing lines, it also gives additional stability of the body during the entire lowering operation. As the transverse (roll) and longitudinal (pitch) GMs might be different due to non-axisymmetric arrangement of wrap buoys during the sequential lowering processes as illustrated in Table 1, the smallest GM values are given in Table 4. The calculation for the KB (keel to center of buoyancy) and the second moment of waterplane area during different stages and different rotational axes are summarized in Appendix**.**

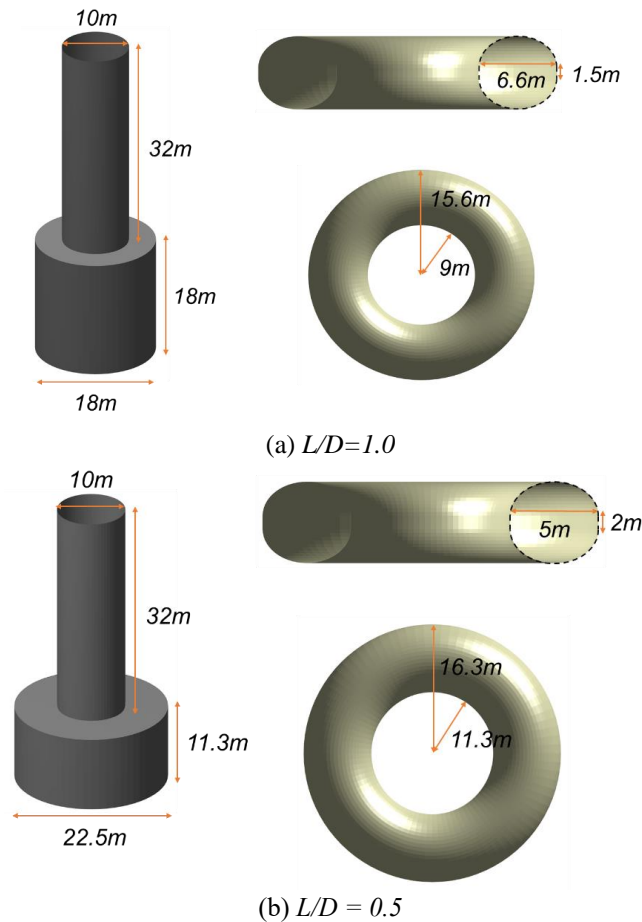(a) *L/D=1.0*

(b) *L/D = 0.5*

Fig. 7 Slender and wide Mono-buckets and the corresponding wrap buoys

The GMs and drafts tabulated here are the values that exclude the towline tensions and the buoyancy from the bucket's wall and lid thickness as their contributions are slight in the intact stability. But they are all considered in the dynamic lowering simulation for double checking. In Table 4, we can observe that there is a significant increase of draft from stage 4 to 5. This is because the remaining two wrap buoys are fully submerged at the equilibrium position of stage 5 (See Table 1), so additional buoyancy after that is only from the increase of tower submergence. For this reason, the transient response becomes considerable and thus the transient dynamic simulation of the stage 4 to 5 is illustrated in Fig. 12 as the worst case scenario.

Wave-induced motion statistics

The wave-induced motion statistics are evaluated by using the generated energy spectrum and the RAOs calculated by program WAMIT. The generated hydrodynamic mesh at the wet-tow position is visualized in Fig. 8 and the WAMIT inputs for the RAO calculations are detailed in Table 5. The heave and pitch motion RAOs are shown in Fig. 9. Also, the corresponding motion spectra

Table 3 Principal dimension of mono-buckets

Monopile	Height (m)	32	
	Diameter (m)	10	
	Thickness (m)	0.95	
	Density (kg/m^3)	7900	
	Mass (Kiloton)	0.75	
	Center of Mass (m)	-14	
Bucket	L/D	1	0.5
	Length, L (m)	18	11.3
	Diameter, D (m)	18	22.5
	Thickness(m)	0.10	0.11
	Mass (Kiloton)	1.01	1.03
	Center of Mass (m)	-37.2	-33.8
Wrap buoys	Inner radius (m)	9	11.3
	Outer radius (m)	15.6 (9 + 2×3.3)	16.3 (11.3 + 2×2.5)
	(Section) radius	3.3	2.5
	(Section) vertical height	1.5	2

Table 4 Intact stability in the lowering operation (L/D=1.0)

Stages	d (m)	BM (m)	z_B (m)	z_G (m)	GM (m)
1 (Towing)	11	24.09	-1.76	9.75	12.58
2 (Lower shackles released)	18.7	24.38	-1.67	2.08	20.63
3 (6 buoys)	19.57	12.93	-2.07	1.17	9.69 (lowest)
4 (4 buoys)	21.23	10.36	-3.10	-0.48	7.74 (lowest)
5 (2 buoys)	29.01	0.29	-7.86	-8.26	0.68
6 (Seabed)	30	No stability required			

are also given in Fig. 10. The detailed wave and motion statistics are summarized in Table 6. The standard deviations, significant wave(motion) amplitudes, and the most probable extreme wave(motion) amplitudes are given for the applied sea states 4, which can be considered as the roughest sea condition for wet-tow and installation. As can be seen in the heave RAO, the motion at a certain frequency is noticeably low. This tendency is also observed in the case of wrap buoy only forming torus without the bucket foundation. Also, as mentioned earlier, 3% and 5% of critical damping are imposed as a linear equivalent viscous damping for heave and pitch to avoid unrealistically large resonance peaks. Furthermore, due to the presence of inner free surface inside the bucket sidewall, it may cause inner free-surface resonance similar to sloshing. The most probable extreme motion amplitudes are 1.7 m for heave at U=2 m/s and 8.1 degrees for pitch at U=0 m/s. As shown in Table 5, a dipole panel method is used for the numerical modeling of sidewall panel since

it is very thin, for which the ordinary panel method can be problematic. This dipole-distribution option is more robust for those thin walls and also reduces computational time. More details regarding the dipole panel method can be found in (Liang *et al.* 2021, Pan 2022) and references therein.

Table 5 Inputs used for the 3D diffraction/radiation program WAMIT

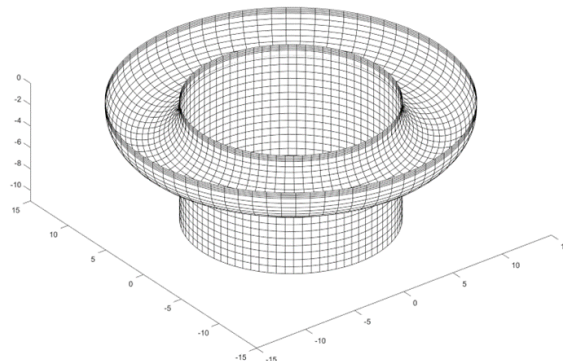| Diameter (m)	18 (bucket) 31.2 (bucket + tube)
Wall thickness (m)	0 (dipole panel)
Mass (Kiloton)	1.76
Center of mass (m)	9.75
Radii of gyration (m)	17.59 ($r_{xx} = r_{yy}$); 7.24 (r_{zz})
Draft (m)	11 (bucket) 4.1 (tube)
Water depth (m)	20
Wave heading (degree)	180 (head sea)

Fig. 8 Hydrodynamics mesh in wet-towing (*L/D*=1.0)
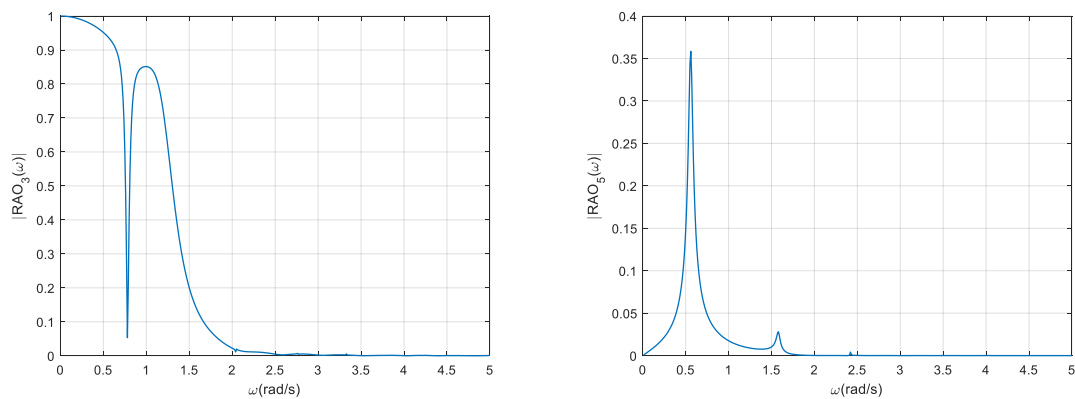

Fig. 9 RAOs (*L/D*=1.0): (left) Heave, (right) Pitch

Table 6 Wave and motion statistics: (*L/D=1.0*)

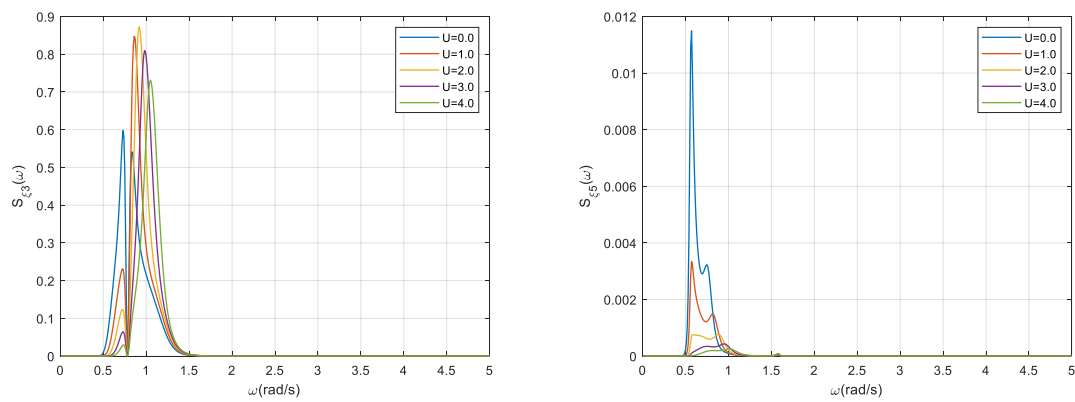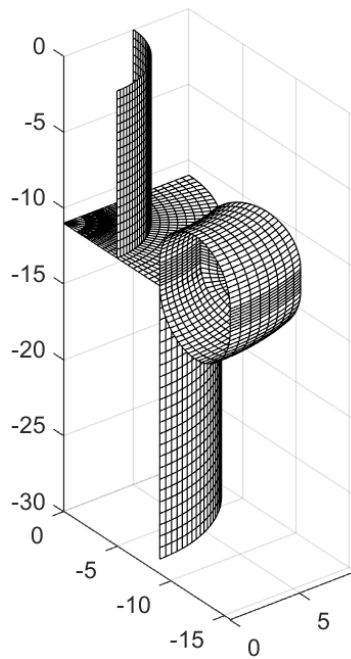| U_{TOW} (m/s)	Wave amplitudes (*m*)			Heave amplitudes (*m*)			Pitch amplitudes (*degree*)		
	σ_ζ	ζ_S	ζ_E	σ_{ξ_3}	$\xi_{3,S}$	$\xi_{3,E}$	σ_{ξ_5}	$\xi_{5,S}$	$\xi_{5,E}$
0.0	0.6256	1.2512	2.4125	0.4245	0.8491	1.6236	2.1577	4.3153	8.0943
1.0	0.6252	1.2505	2.4292	0.4356	0.8711	1.6727	1.4535	2.9070	5.4876
2.0	0.6247	1.2494	2.4424	0.4457	0.8914	1.7172	1.0119	2.0237	3.8496
3.0	0.6241	1.2482	2.4529	0.4392	0.8784	1.6973	0.7497	1.4995	2.8735
4.0	0.6233	1.2467	2.4613	0.4222	0.8444	1.6365	0.5896	1.1792	2.2742

Fig. 10 Motion spectrum (*L/D*=1.0): (left) Heave, (right) Pitch

Fig. 11 Hydrodynamics mesh in the lowering phase (*L/D*=1.0)

Table 7 Specification for the lowering operation (*L/D*=1.0)

Height (*m*)	18 (bucket sidewall); 32 (monopile)
Diameter (*m*)	18 (bucket); 10 (monopile)
Wall thickness (*m*)	0 (dipole panel)
Mass (kiloton)	1.76
Drag coefficients	$C_{D,n}$ =2.5; $C_{D,t}$ =0.008
Tension (*tf*)	100-200
Draft (*m*)	20-30
Water depth (m)	30

Lowering operation

The transient response of the bucket foundation is simulated from the lowering stage 4 to 5. As stated earlier, the added mass and the retardation functions are obtained for various drafts and then interpolated by interpolating polynomial. Specifications for the lowering operation is given in Table 7 and the mesh for the hydrodynamic calculation at the selected stage is illustrated in Fig. 11. The dipole panels are used for the sidewall and top-lid part. The time-series of the transient motion and velocity are shown in Fig. 12. The Additional buoyancy due to the thickness of the bucket is additionally included for the simulation. Also, towline tensions are additionally given as in Eq. (6). For the present lowering simulation, the maximum overshoot draft is about 29.7m and the maximum falling velocity is about 0.96 m/s assuming 100tf of towline tension. Thereafter, the transient motions and velocities are significantly reduced by damping. The relevant oscillation period is about 25 seconds and the oscillation velocity is small, so the last remaining two segmented wrap buoys can further be disconnected so that the foundation can finally be mounted on the seabed with the help of line tensions.
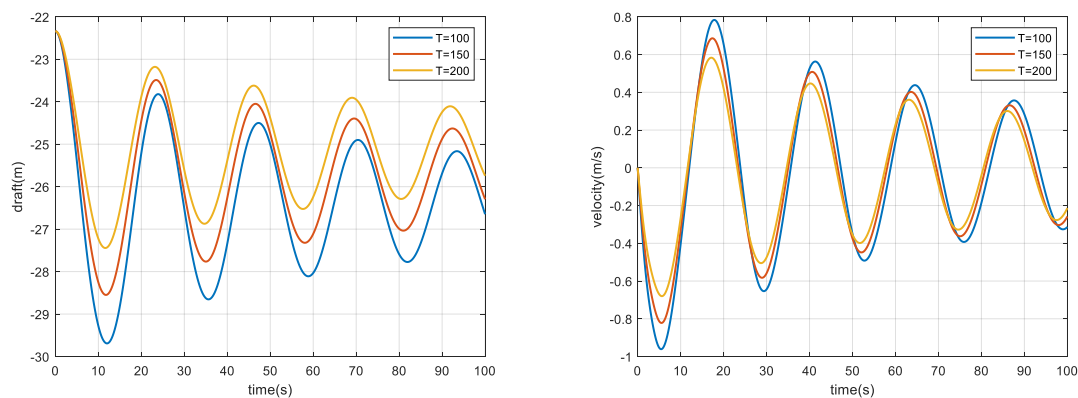
3.3 Case study-2: Wide bucket L/D = 0.5

Intact stability

Compared to the previous slender bucket, a wider (diameter=22.5 m) and less tall (11.3 m) bucket is considered here, which can also provide enough foundation strength for the NREL 15 MW wind turbine. (Aubeny 2022, Aubeny and Aldawwas 2022). From hydrodynamics point of view, the wider bucket provides larger second moment of waterplane area in pitch/roll and larger added mass and viscous drag force in transient falling, and thus it seems hydrodynamically more advantageous. By this reason, the size of the wrap buoys can be smaller compared to the previous case. It also allows initial loadout in a relatively shallow port. In Table 8, the metacentric heights are calculated for all lowering stages. One more last sub-step is added for the present case of *L/D=0.5* so that the bucket can gently land on the seabed. Since the initial draft is smaller, the vertical travel distance needed to be lowered down becomes longer than the former case. In this regard, we split the last step into two sub-steps, so that we can further reduce the transient response. On the other hand, one can see that there is a temporarily negative GM in the stage 5. This issue can easily be resolved by adjusting the attachment height of wrap buoys up by 2.5 m which leads to the GM increase about 1 m. Also, the additional restoring moment from the three towlines further increases the GM value.

Table 8 Intact stability in the lowering operation (*L/D=0.5*)

Stage	d (m)	BM (m)	z_B (m)	z_G (m)	GM (m)
1 (Towing)	10	24.5344	-2.0431	10.9058	11.5855
2 (Lower shack released)	13.0313	24.8169	-1.8094	2.8745	20.1329
3 (6 buoys)	14.0318	12.5634	-2.3852	1.8740	8.3042 (lowest)
4 (4 buoys)	15.5804	5.1771	-3.6904	0.3254	1.1612 (lowest)
5 (2 buoys)	23.5925	0.2825	-8.8105	-7.6867	-0.8418
6 (1 buoy or 2 half buoys)	27.6822	0.2825	-10.4350	-11.7763	1.6238
7 (Seabed)	30	No stability required			

Fig. 12 Time series of transient motions between stage 4 and 5: (left) draft change, (right) heave velocity (*L/D*=1.0)
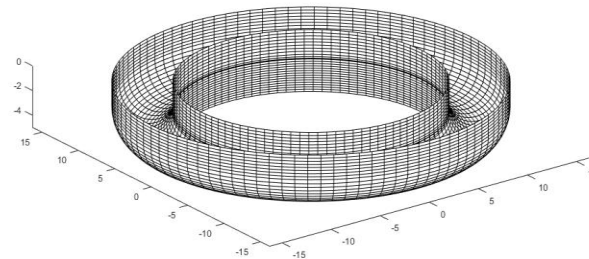
Wave-induced motion statistics

The specification for wet-towing is given in Table 9 and hydrodynamics mesh is illustrated in Fig. 13. The wrap buoys are tightly connected to the sidewall pad-eyes so that its center line coincides with the bucket tow draft of 5 m. The same sea state 4 is applied. Heave and pitch RAOs are shown in Fig. 14 and the corresponding motion spectra are presented in Fig. 15. Typical motion statistics are tabulated in Table 10. In the present case, the highest motion amplitudes are at zero tow speed for both heave and pitch motions. The most probable extreme motion amplitude for heave is 1.8 m whereas 10.1 degrees for pitch. Both maximum heave and pitch amplitudes are slightly increased compared to the previous slender and taller bucket due to decreased viscous damping by smaller wrap buoys and shallower bucket draft. The performance comparisons between the two different bucket dimensions are made in Section 3.3 in more detail.

Table 9 Specification for wet-towing (*L/D*=0.5)

Diameter (m)	22.5 (bucket) 32.5 (bucket + tube)
Wall thickness (m)	0 (dipole panel)
Mass (Kiloton)	1.78
Center of mass (m)	10.75
Radii of gyration (m)	17.16 ($r_{xx} = r_{yy}$); 8.48 (r_{zz})
Draft (m)	5 (bucket) 4.5 (tube)
Water depth (m)	20
Wave heading (degree)	180 (head sea)

Table 10 Wave and motion statistics: (*L/D*=0.5)

U_{TOW} (*m/s*)	Wave amplitudes (*m*)			Heave amplitudes (*m*)			Pitch amplitudes (*degree*)		
	σ_ζ	ζ_S	ζ_E	σ_{ξ_3}	$\xi_{3,S}$	$\xi_{3,E}$	σ_{ξ_5}	$\xi_{5,S}$	$\xi_{5,E}$
0.0	0.6256	1.2512	2.4125	0.4797	0.9595	1.8272	2.6912	5.3823	10.1104
1.0	0.6252	1.2505	2.4292	0.4275	0.8550	1.6366	1.8713	3.7426	7.0600
2.0	0.6247	1.2494	2.4424	0.3603	0.7206	1.3863	1.2904	2.5807	4.8997
3.0	0.6241	1.2482	2.4530	0.3067	0.6134	1.1867	0.9120	1.8240	3.4930
4.0	0.6233	1.2467	2.4613	0.2971	0.5943	1.1553	0.6897	1.3793	2.6658

Fig. 13 Hydrodynamics mesh in wet-towing (*L/D=0.5*)

Lowering operations

The transient response of the bucket foundation is simulated for the worst possible case i.e., between stage 5 to 6 in Table 8. As mentioned earlier, the stage 6 is a sub-step in which two half-length wrap tubes are used. The specification for the lowering operation is summarized in Table 11 and the hydrodynamics mesh used at the stage 5 is visualized in Fig. 16. The time series of the instantaneous draft and oscillatory vertical velocity during the transient motion are shown in Fig. 17. For the present simulation, the maximum overshoot draft is about 29 m and the maximum falling velocity is about 0.67 m/s assuming 100tf of towline tension. The vertical fall velocity is generally reduced compared to the previous slender bucket case so that the final stage near the seabed becomes safer.
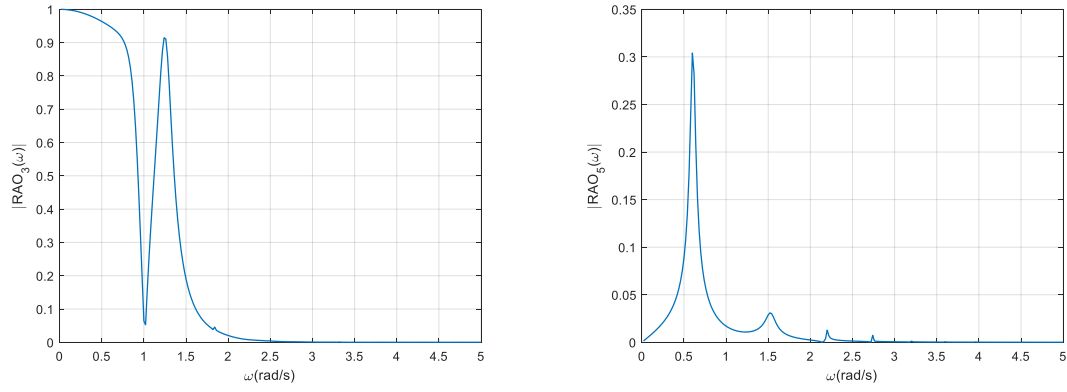
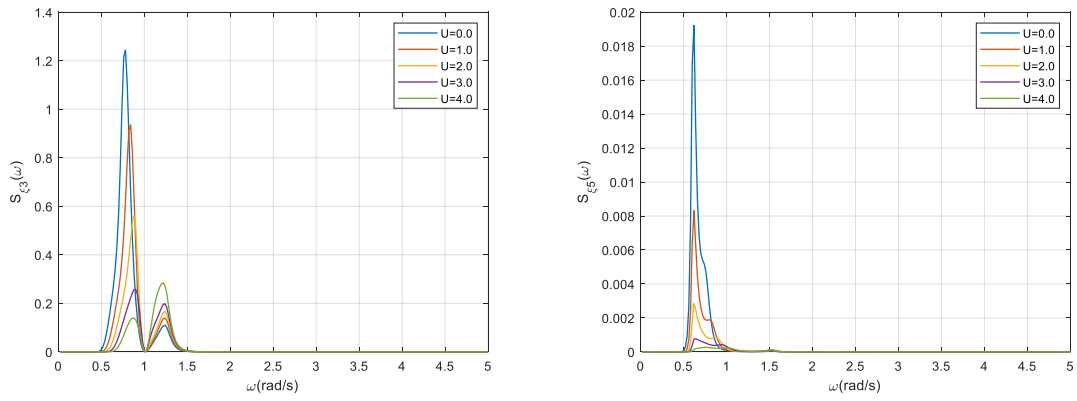Fig. 14 RAOs (*L/D*=0.5): (left) Heave, (right) Pitch

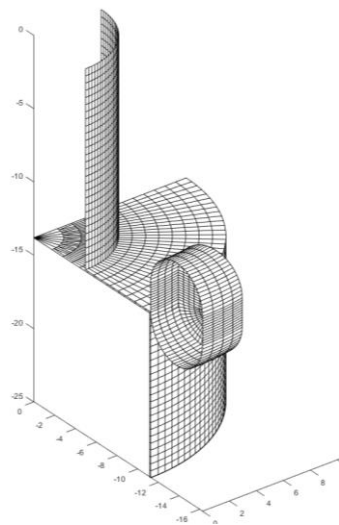Fig. 15 Motion spectrum (*L/D*=0.5): (left) Heave, (right) Pitch

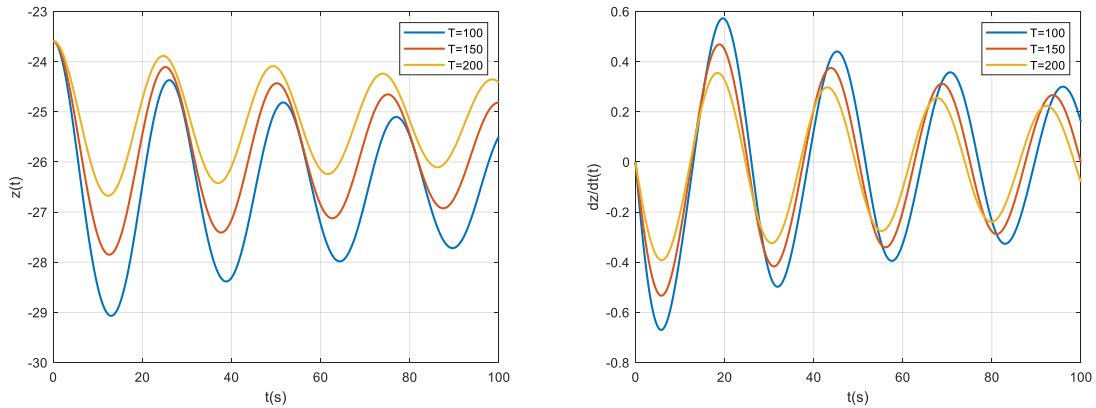Fig. 16 Hydrodynamic mesh in the lowering phase (*L/D*=0.5)

Fig. 17 Time series of transient motions between stage 5 and 6: (left) draft change, (right) heave velocity (*L/D*=0.5)

3.3 Hydrodynamic performance comparisons: L/D=1.0 vs L/D=0.5

The performance comparison between the two different bucket and wrap-buoy dimensions is made and summarized in Table 12. Firstly, regarding the intact stability during sequential installation, the wider bucket temporarily experienced small negative GM, which can be remedied by slightly raising the initial wrap-buoy connection point or through cable tensions from 3 tug-boats. However, in the wet-towing stage, the wider bucket has better stability and smaller resistance with lower draft, which is also important for the load out in a shallow port. On the other hand, the motion amplitudes of the wider bucket under the same sea state 4 are slightly larger compared to the slender and taller bucket. The increased bucket draft tends to reduce the pitch motion but may increase tow resistance. For the lowering operation, the wider bucket reduces transient motion and velocity amplitudes, which leads to higher overall safety. In general, more segments of wrap buoys can make the overall installation process milder and safer. However, it requires more acoustic shackles and connection cables and thus higher manufacturing cost. Also, water ballasting of the last remaining wrap buoys at the last stage is also possible for more gradual sinking near the seabed. As soon as the bucket is properly seated on the seabed, the suction pump can pump out the inside water so that the external hydrostatic pressure can further push the bucket into the soil. As expected, the wider bucket has better resistance against the wave-induced overturning moment when seated on the seabed, as shown in Table 12. The Morison equation overestimates the overturning moment. This is due to the fact that the hydrodynamic pressure acting on the top-lid of the bucket (Eq. (15)), not considered in the Morison equation, reduces the overturing moment. After the bucket foundation is fully penetrated into the soil, the full assembly of upper part of wind turbine can be mated by using float-over installation vessel. Additionally, the maximum shackle tension was calculated for *L/D=1.0* based on the lowering simulation result and it amounts to 250tonne. This is within the range of load capacity of available acoustic shackles (e.g., Applied Acoustic Engineering Ltd.). During the stepwise lowering operation, maximum transient responses and velocities of wider/shallower bucket are smaller thus safer compared to those of slender bucket. When seated on the seabed, the resistance of wider bucket against wave-induced overturning moment is better than that of slender bucket.

Table 12 Comparison between two different bucket dimensions: *L/D = 1.0 vs 0.5*

Dimension	L/D	1.0	0.5
Intact stability	Minimum GM	0.68 at step 5 (2 wrap buoys left)	-0.84 at step 5 (2 wrap buoys left)
Extreme motion amplitudes (3hrs)	Heave (m)	1.7 (*U=2 m/s*)	1.8 (*U=0 m/s*)
	Pitch (degree)	8.1 (*U=0 m/s*)	10.1 (*U=0 m/s*)
Lowering operation	Maximum draft	29.7 (*100tf*)	29.1 (*100tf*)
	Maximum vel.	0.96	0.67
Overturning moment	$\mu(= M_{over,max}/M_{res})$	0.68 (2D Morison) 0.63 (3D Diffract.)	0.46 (2D Morison) 0.41 (3D Diffract.)

4. Conclusions

Feasibility study for innovative wet-towing and stepwise-installation solutions of mono-bucket foundation for 15 MW offshore wind turbine was carried out. The intact stability and hydrodynamic performance were investigated for two selected (slender/tall vs wider/less height) bucket sizes. In particular, the intact stability in all the towing and lowering stages, wave-induced motion statistics during wet-towing in sea state 4, transient-response in stepwise lowering process, and overturning moment at seabed-seated instant were analyzed. Also, systematic performance comparisons between the two selected bucket dimensions were made. Both cases worked well for wet-tow and stepwise installation and wider bucket had the advantage in smaller transient responses during stepwise lowering as well as smaller wet-tow resistance and launching in shallower port due to smaller draft. Based on the numerical results, it was concluded that the suggested concept is feasible as a new method for the vertical wet-tow and efficient installation of suction bucket foundation without using heavy-lift crane vessels. The same methodology can in principle be applied to a jacket foundation with multiple smaller suction buckets. To further validate the proposed concepts, scaled experiments and comparisons with the developed numerical simulations are planned as the next research.

Acknowledgments

References

Abdel-Rahman, K. and Achmus, M. (2006), "Behaviour of monopile and suction bucket foundation systems for offshore wind energy plants", *Proceedings of the 5th International Engineering Conference*, Sharm El-Sheikh, Egypt.

Applied Acoustic Engineering Ltd., "Wireless acoustic load shackle system", https://www.aaetechnologiesgroup.com/wp-content/uploads/2021/02/Wireless-Acoustic-Load-Shackle-–-Technical-Specification-Issue-1.pdf.

Aubeny, C.P. (2022), "Simulate suction installation", prepared for New York State Energy Research and Development Authority, Project 106, Vibratory-Installed Bucket Foundation for Fixed Foundation Offshore Wind Towers, Texas Engineering Experiment Station, College Station, Texas.

Aubeny, C.P. and Aldawwas, A. (2022), "Phase 1 comparative evaluation of installation methods", prepared for New York State Energy Research and Development Authority, Project 106, Vibratory-Installed Bucket Foundation for Fixed Foundation Offshore Wind Towers, Texas Engineering Experiment Station, College Station, Texas.

Det Norske Veritas (2000), "DNV-RP-H103 modelling and analysis of marine operations", Det Norske Veritas, Høvik, Oslo, Norway.

Esteban, M.D., Counago, B., Lopez-Gutierrez, J.S., Negro, V. and Vellisco, F. (2015), "Gravity based support structures for offshore wind turbine generators: Review of the installation process", *Ocean Eng.*, **110**, 281-291. https://doi.org/10.1016/j.oceaneng.2015.10.033.

Esteban, M.D., Lopez-Gutierrez, J.S. and Negro, V. (2019), "Gravity-based foundations in the offshore wind sector", *J. Mar. Sci. Eng.*, **7**(3), 64. https://doi.org/10.3390/jmse7030064.

Feld, T. (2001), "Suction Buckets: a new innovation foundation concept, applied to offshore wind turbines".

Fiorentino, L.A., Heitsenrether, R., Teng, C.C. and Muglia, M. (2019), "Field test results from ellipsoid ADCP buoy moored at the edge of the gulf stream", 2019 IEEE/OES Twelfth Current, Waves and Turbulence Measurement (CWTM).

Gaertner, E., Rinker, J., Sethuraman, L., Zahle, F., Anderson, B., Barter, G., Abbas, N., Meng, F., Bortolotti, P., Skrzypinski, W., Scott, G., Feil, R., Bredmose, H., Dykes, K., Shields, M., Allen, C. and Viselli, A. (2020), "Definition of the IEA 15-megawatt offshore reference wind turbine", National Renewable Energy Laboratory: Golden, Colorado, USA.

Hasselmann, K. and Olbers, D. (1973), "Measuremeants of wind-wave growth and swell decay during the Joint North Sea Wave Project (JONSWAP)", *Ergänzung zur Deut. Hydrogr. Z., Reihe A*, **12**, 1-95.

Huang, L., Zhang, J., Yu, X., Randall, R.E. and Wilde, B. (2011), "Numerical simulation on dynamics of suction piles during lowering operations", *Proceedings of the 21st International Offshore and Polar Engineering Conference*, Maui, Hawaii, USA.

Jang, H.K. and Kim, M.H. (2019), "Mathieu instability of arctic spar by nonlinear time-domain simulations", *Ocean Eng.*, **176**, 31-45. https://doi.org/10.1016/j.oceaneng.2019.02.029.

Jeong, Y.H., Ko, K.W., Kim, D.S. and Kim, J.H. (2021), "Studies on cyclic behavior of tripod suction bucket foundation system supporting offshore wind turbine using centrifuge model test", *Wind Energy*, **24**(5), 515-529. https://doi.org/10.1002/we.2586.

Jiang, Z. (2021), "Installation of offshore wind turbines: A technical review", *Renew. Sust. Energ. Rev.*, **139**, 110576. https://doi.org/10.1016/j.rser.2020.110576.

Journée, J.M. and Massie, W. (2001), Offshore hydromechanics, Delft University of Technology Delft

Lee, C.H. (1995), "WAMIT theory manual", Department of Ocean Engineering, Massachusetts Institute of Technology, Cambridge, MA, USA.

Lian, J., Ding, H., Zhang, P. and Yu, R. (2012), "Design of large-scale prestressing bucket foundation for offshore wind turbines", *Trans. Tianjin Univ.*, **18**, 79-84. https://doi.org/10.1007/s12209-012-1661-5.

Liang, H., Shao, Y. and Chen, J. (2021), "Higher-order derivatives of the Green function in hyper-singular integral equations", *Eur. J. Mech.-B/Fluid.*, **86**, 223-230. https://doi.org/10.1016/j.euromechflu.2020.12.006.

Mazzaretto, O.M., Menéndez, M. and Lobeto, H. (2022), "A global evaluation of the JONSWAP spectra suitability on coastal areas", *Ocean Eng.*, **266**, 112756. https://doi.org/10.1016/j.oceaneng.2022.112756.

Orcina Ltd., "Payload handling: F07 Suction anchor lowering", https://www.orcina.com/wp-content/uploads/examples/f/f07/F07%20Suction%20anchor%20lowering.pdf.

Pan, Z. (2022), "Application of a BEM model with dipole elements", *Ocean Eng.*, **249**, 110938. https://doi.org/10.1016/j.oceaneng.2022.110938.

Sundt, R.C., Børseth, J.F. and Myhre, L.P. (2009), "A simple acoustic release trap system for live capture of deep-water organisms", Marine Biodiversity Records, 2.

Wang, X.F., Zeng, X.W. and Li, J.L. (2019), "Vertical performance of suction bucket foundation for offshore wind turbines in sand", *Ocean Eng*., **180**, 40-48. https://doi.org/10.1016/j.oceaneng.2019.03.049.

Weisstein, Eric W. "Gill's Method" From MathWorld--A Wolfram. https://mathworld.wolfram.com/GillsMethod.html.

Wu, J. and Kim, M.H. (2021), "Generic upscaling methodology of a floating offshore wind turbine", *Energies J.*, **14**, 8490. https://doi.org/10.3390/en14248490.

Zhang, P., Han, Y., Ding, H. and Zhang, S. (2015), "Field experiments on wet tows of an integrated transportation and installation vessel with two bucket foundations for offshore wind turbines", *Ocean Eng.*, **108**, 769-777. https://doi.org/10.1016/j.oceaneng.2015.09.001.

PS

Appendix A

Intact stability in lowering stages

The intact stability in the lowering stages can be calculated by Eq. (1). In the formula, z_G is determined by $z_G = KG - d$; d is instantaneous draft shown in Fig. 5, and KG is fixed value. On the contrary, $z_B (= KB - d)$ and $BM (= I_{xx(yy)}/\nabla)$ are varying according to the change of draft and wetted geometry. Here, KB and values for partially submerged wrap tubes are given in Table A-1 (stages 2-4), and the second moment of waterplane areas are in Table A-2 (stages 3-4).

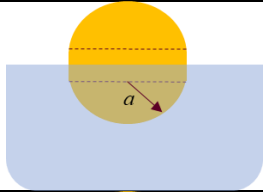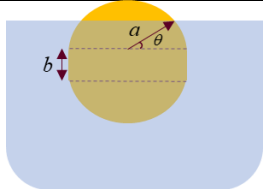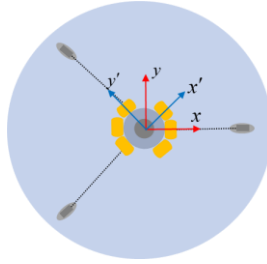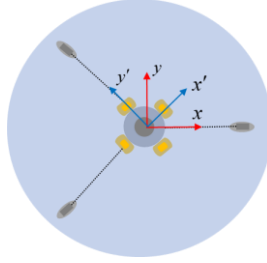Table A-1. KBs for partially submerged wrap buoys (stages 2-4)

Section view	KB
	$$\dfrac{\pi a^2\left(a - \dfrac{4a}{3\pi}\right) + 2ah(2a + h)}{\pi a^2 + 4ah}$$
	$$\dfrac{3\left(a^3 + a^2 b\right)(2\theta + \sin 2\theta) + a^3\left(3\pi - 4\cos^3\theta\right) + \left(12a^2 b + 6ab^2\right)}{3a^2\left(2\theta + \pi + \sin 2\theta\right) + 12ab}$$

Table A-2 Non-axisymmetric second moment of waterplane area (stages 3-4)

Section view	$I_{xx}, I_{yy}, I_{x'x'}, I_{y'y'}$
	$$I_{xx} = \frac{\left(3\pi + 2\sqrt{2}\right)\left[\left(R + a + a\cos\theta\right)^4 - \left(R + a - a\cos\theta\right)^4\right]}{16}$$ $$I_{yy} = \frac{\left(3\pi - 2\sqrt{2}\right)\left[\left(R + a + a\cos\theta\right)^4 - \left(R + a - a\cos\theta\right)^4\right]}{16}$$ $$I_{x'x'} = I_{y'y'} = \frac{3\pi\left[\left(R + a + a\cos\theta\right)^4 - \left(R + a - a\cos\theta\right)^4\right]}{16}$$
	$$I_{xx} = I_{yy} = I_{x'x'} = I_{y'y'} = \frac{\pi\left[\left(R + a + a\cos\theta\right)^4 - \left(R + a - a\cos\theta\right)^4\right]}{8}$$